HHS Public Access

Author manuscript

Cell Rep. Author manuscript; available in PMC 2022 June 06.

Published in final edited form as:

Cell Rep. 2022 May 17; 39(7): 110826. doi:10.1016/j.celrep.2022.110826.

T cell transcription factor expression evolves over time in granulomas from *Mycobacterium tuberculosis*-infected cynomolgus macaques

Nicole L. Grant[1], **Pauline Maiello**[2], **Edwin Klein**[3], **Philana Ling Lin**[4,5], **H. Jacob Borish**[2], **Jaime Tomko**[2], **L. James Frye**[2], **Alexander G. White**[2], **Denise E. Kirschner**[6], **Joshua T. Mattila**[1,5], **JoAnne L. Flynn**[2,5,7,*]

[1]Department of Infectious Diseases and Microbiology, Graduate School of Public Health, University of Pittsburgh, Pittsburgh, PA, USA

[2]Department of Microbiology and Molecular Genetics, University of Pittsburgh School of Medicine, University of Pittsburgh, Pittsburgh, PA, USA

[3]Division of Laboratory Animal Research, University of Pittsburgh, Pittsburgh, PA, USA

[4]Department of Pediatrics, Children's Hospital of Pittsburgh of the University of Pittsburgh Medical Center, Pittsburgh, PA, USA

[5]Center for Vaccine Research, University of Pittsburgh, Pittsburgh, PA, USA

[6]Department of Microbiology and Immunology, University of Michigan Medical School, Ann Arbor, MI, USA

[7]Lead contact

SUMMARY

Mycobacterium tuberculosis (Mtb), the causative agent of tuberculosis (TB), is a global health concern, yearly resulting in 10 million new cases of active TB. Immunologic investigation of lung granulomas is essential for understanding host control of bacterial replication. Here, we identify and compare the pathological, cellular, and functional differences in granulomas at 4, 12, and 20 weeks post-infection in Chinese cynomolgus macaques. Original granulomas differ in transcription-factor expression within adaptive lymphocytes, with those at 12 weeks showing higher frequencies of $CD8^+$T-bet^+ T cells, while $CD4^+$T-bet^+ T cells increase at 20 weeks post-infection. The appearance of T-bet^+ adaptive T cells at 12 and 20 weeks is coincident with a

*Correspondence: joanne@pitt.edu.

AUTHOR CONTRIBUTIONS

Conceptualization, J.L.F. and D.E.K.; investigation, N.L.G., E.K., H.J.B., A.G.W., and P.M.; resources, J.T., E.K., L.J.F., J.T.M., and P.L.L.; formal analysis, N.L.G., P.M., and J.L.F.; writing – original draft, N.L.G. and J.L.F.; writing – review & editing, N.L.G., P.M., H.J.B., E.K., P.L.L., J.T.M., and D.E.K.; visualization, N.L.G., P.M., and E.K.; supervision, J.L.F. and J.T.M.; funding acquisition, J.L.F. and D.E.K.

DECLARATION OF INTERESTS

Authors from the University of Pittsburgh and University of Michigan have no competing interests.

SUPPLEMENTAL INFORMATION

Supplemental information can be found online at https://doi.org/10.1016/j.celrep.2022.110826.

reduction in bacterial burden, suggesting their critical role in *Mtb* control. This study highlights the evolution of T cell responses within lung granulomas, suggesting that vaccines promoting the development and migration of T-bet^{+} T cells would enhance mycobacterial control.

Graphical Abstract

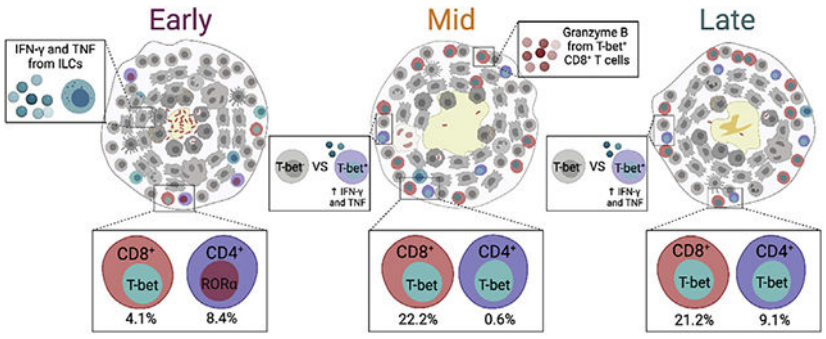

In brief

Grant et al. investigate the pathological, cellular, and functional differences in TB lung granulomas from macaques. The data reveal that most T cells at early time points have low frequencies of transcription factor expression, while T cells at later time points have increased expression of T-bet and a reduction in bacterial burden.

INTRODUCTION

Mycobacterium tuberculosis (Mtb), the etiologic agent of tuberculosis (TB), has caused considerable morbidity and mortality for thousands of years (Barberis et al., 2017). Due to the coronavirus 2019 (COVID-19) pandemic, TB mortality is estimated to increase despite headway made in recent years by the End TB Strategy (WHO, 2020). There are still many unanswered questions about interactions of *Mtb* with its human host, and understanding these interactions is critical to the development of improved treatments and preventive strategies. The complexity of TB disease is highlighted in the intricate pathological structure that forms following inhalation of *Mtb* bacilli, the lung granuloma. This dynamic structure is comprised of both innate and adaptive immune cells, and it undergoes cellular and molecular fluctuations throughout the course of infection leading to disparate trajectories, with some restricting or killing bacilli and others exhibiting a failure in bacterial control, propagating dissemination, and progressive disease.

Despite extensive research, the immunological contributors to bacterial control in granulomas are not well understood. Studies investigating the role of adaptive T cells in *Mtb*-infected mice have revealed interferon gamma (IFN-γ)-dependent and -independent mechanisms of control, suggesting that these cells have other critical functions in limiting TB disease (Kumar, 2017; Green et al., 2013; Gallegos et al., 2011). The influence of transcription factor (TF) expression, as a surrogate for immune cell function, has been studied in mice infected with *Mtb*, revealing a protective phenotype related to expression of the pro-inflammatory TF T-bet (Sullivan et al., 2005). This is supported by studies in

human patients with Mendelian susceptibility to mycobacterial disease (MSMD), which can be caused by defects in the genes encoding T-bet (*TBX21*) and RORγT (*RORC*) (Okada et al., 2015; Yang et al., 2020). A better understanding of TF expression within the context of the granuloma would enhance our ability to interpret T cell function in TB.

Investigating granuloma function in human TB disease is limited due to difficulty in obtaining representative samples, lack of data regarding time of infection, variable treatments, and little microbiologic information, necessitating the use of an animal model. Whereas many models for TB exist, non-human primates (NHPs) are invaluable as they reflect the range in granuloma pathology seen in humans (Capuano et al., 2003; Lin et al., 2009). Cynomolgus macaques infected with virulent *Mtb* strains have been particularly useful as they recapitulate the full spectrum of infection outcomes seen in humans ranging from controlled (latent infection) to active TB disease (Lin et al., 2009, 2014; Maiello et al., 2017). We track granuloma formation following *Mtb* infection through positron emission tomography and computed tomography (PET CT) using ^{18}F-fluorodeoxyglucose (FDG) as a PET probe, which incorporates into metabolically active host cells within granulomas (White et al., 2017; Coleman et al., 2014a, 2014b; Lin et al., 2013). Serial PET CT scans over the course of infection provide a history for individual granulomas including time of detection, location, and changes in size and FDG avidity (Coleman et al., 2014b; White et al., 2017). Understanding the timing of granuloma formation is critical, as granulomas observed at 4 weeks post-infection (termed original granulomas) represent those that are established by individual *Mtb* bacilli from the inoculum (Martin et al., 2017). Previous data indicate that granulomas that develop at later time points post-infection (new granulomas), either through dissemination or slower growth of *Mtb*, have different features as they arise during an ongoing immune response, resulting in a decreased bacterial burden (Gideon et al., 2022; Lin et al., 2014). Differences in bacterial burden are also observed throughout the course of infection in granulomas; although the immune mechanisms responsible for this reduction in bacterial burden remain unclear, it likely relates to the evolving immunological state of the granuloma (Lin et al., 2014).

The present study is the first to investigate the interplay of TFs and bacterial dynamics in original NHP lung granulomas throughout the course of infection. We aimed to evaluate the cellular and functional changes in original granulomas over time using samples from macaques necropsied at early (4 weeks), mid (12 weeks), and late (20 weeks) time points post-infection. We observed temporal differences in TF expression in adaptive lymphocytes that correlate with bacterial burden, providing insight into the evolution of TB lung granulomas over time. These data suggest that protective adaptive immune responses are slow to develop and are coincident with a reduced bacterial burden in granulomas at later time points post-infection.

RESULTS

Study design and granuloma dynamics in original granulomas

To assess temporal changes in cellular composition, structure, and function of granulomas, 8 cynomolgus macaques were infected with a low dose of virulent *Mtb* and necropsied at 4 (N = 2), 12 (N = 3), or 20 (N = 3) weeks, representing early, mid, and late time points

post-infection (Figure 1A). Granuloma formation was tracked over time using serial PET CT imaging starting at 4 weeks post-infection, with PET CT scans performed every 2 to 4 weeks for the duration of the study. Based on these scans, we identified 94 original granulomas as those first observed on a 4-week scan that were individually harvested at necropsy and homogenized to a single-cell suspension, which was used for colony-forming unit (CFU) quantification and flow cytometry. For granulomas >2 mm, a portion was fixed in formalin for histology. In this study, our focus was on granuloma cellular composition, structure, and functional changes over time using only original granulomas. Consistent with previous data, original granulomas at 4 weeks post-infection had significantly higher CFUs, but a similar size as measured by PET CT, when compared with original granulomas harvested at mid and late time points (Figure 1B) (White et al., 2017; Lin et al., 2014).

Histopathology and cellular spatial arrangement of original granulomas

Lung granulomas from *Mtb*-infected macaques are structurally similar to granulomas found in human TB patients (Flynn et al., 2015). Spatial arrangement is likely to be important for immune interactions and bacterial containment; thus, we compared the histological and spatial differences in original granulomas at early, mid, and late time points post-infection (Millar et al., 2020). In addition to samples from the monkeys dedicated to this study, we supplemented with banked samples of original granulomas isolated from monkeys at similar time points post-infection. The majority of original granulomas in individual animals had necrotic features, though lower frequencies of necrotic original granulomas were observed at the late time point compared with the early time point (Figure 1C). Necrotic or caseous features in granulomas can be observed in conjunction with other histologic findings such as fibrosis, collagenization, or mineralization (Flynn and Klein, 2011; Capuano et al., 2003). While these secondary components were occasionally seen in original granulomas at the early time point, they were observed more frequently in original granulomas at the mid and late time points, suggesting that they are temporally related to the transitional granuloma environment (Figure 1C). A range of histopathological classifications (as defined by our pathologist, Edwin Klein) were also seen in original granulomas at all time points including classically necrotic, as well as rarer pathologies, such as evolving necrosis, early collagenization, fibrocalcific, and granuloma scarring (Figure S1C). We compared the CFUs of fibrotic versus non-fibrotic granulomas from the mid and late time points and observed improved bacterial control in granulomas with fibrosis compared with non-fibrotic granulomas (Figure S1A), consistent with previous data (Lin et al., 2014).

While original granulomas at 12 and 20 weeks have reduced CFUs compared with those at 4 weeks, sterilization of original granulomas from animals in this study and banked samples was rare at all time points, with the highest proportion at late time points (Figure S1B). Furthermore, sterile granulomas from the mid and late time points had split classifications based on histologic components, with some being fibrotic, neutrophilic, collagenic, or classically necrotic (Figure S1B). Classic necrotic granulomas are structurally organized, having a central caseous core surrounded by concentric rings of epithelioid macrophages and lymphocytes (Flynn et al., 2011; Flynn and Klein, 2011). With the exception of secondary structural elements (i.e., mineralization, fibrosis), visual comparison of H&E-stained original necrotic granulomas from different time points revealed no distinct differences in

overall granuloma structure (Figure 1D). We assessed this typical granuloma structure using immunofluorescently stained tissue sections for $CD3^+$, $CD11c^+$, and $CD163^+$, finding more clusters of $CD11c^+$ cells in granulomas from the early and mid time points. These clusters may be a precursor to the typically observed macrophage ring, suggesting that timing plays a role in the development of cellular spatial compartments in granulomas (Figure 1D).

Cellular composition in original lung granulomas over time

Granulomas are dynamic structures composed of lymphoid and myeloid cells that contribute to bacterial control. We and others have previously reported substantial heterogeneity in granulomas in individual macaques and across macaques (Capuano et al., 2003; Lin et al., 2014; Gideon et al., 2015; Maiello et al., 2017). Here, we investigated whether there were differences in overall cellular composition in 94% of the original granulomas (88 of the 94) identified by PET CT using flow cytometry (Figure S2). A higher overall adjusted cell count (see STAR Methods) was observed at the early time point for both myeloid and lymphocyte populations, whereas frequencies of these cell types were similar across all time points (Figures 2A and S3A). There were no significant differences in the frequency of $CD3^+$ cells across time points, but there were significantly higher frequencies of $CD20^+$ B cells at the mid time point and significantly higher frequencies of $CD3^-CD20^-$ cells (including natural killer [NK] and other innate lymphocytes) at the late time point (Figure 2C). Further analysis into $CD3^+$ subsets revealed significantly lower frequencies of $CD4^+$ T cells at the mid compared with the late time point (medians: mid, 19.69%; late, 24.39%; p value, 0.0297) and significant differences in the frequencies of $CD8^+$ T cells at each time point, with the highest levels being at the mid time point (medians: early, 17.36%; mid, 27.46%; late, 20.26%; $p < 0.0001$ for early to mid, 0.0161 for mid to late, and 0.0112 for early to late) (Figures 2B-2D). We observed low frequencies of both $CD3^+CD4^-CD8^-$ and $CD3^+CD4^+CD8^+$ cells at all time points, with the highest median frequency for both cell types at the early time point (median: 4.81% and 4.95%, respectively) (Figures 2B and 2D).

Myeloid cells make up approximately 25% of the cells in original granulomas regardless of time point (Figure S3A); since there were more cells in early granulomas, these samples also had the highest adjusted myeloid cell count. At the early time point, there were higher frequencies of $CD11c^+$, $CD11b^+$, and $CD163^+$ myeloid cells in granulomas (Figures S3B and S3C). To evaluate functional differences in myeloid cells, we compared the frequency of these cells producing interleukin (IL)-10, tumor necrosis factor (TNF), and IFN-γ. While the frequencies of myeloid cells expressing any of the cytokines investigated was very low, there were significantly higher levels of IL-10 and IFN-γ in the late time point compared with the mid and early time points and significantly lower levels of TNF at the mid time point compared with the early time point (Figure S3D).

TF expression increases in granuloma adaptive T cells at 12 and 20 weeks post-infection

T cells are known to be important for controlling *Mtb*; however, the breadth in function of these cells within lung granulomas remains incompletely studied. Our data (Figure 2C) and previous data suggest that although $CD3^+$ cells make up approximately half of all cells in the granuloma (medians: 50.63%–53.78%) across time points, very few are reportedly producing cytokines within the granuloma (Gideon et al., 2015; Wong et al., 2018; Phuah

et al., 2016; Millar et al., 2020). In this study, we analyzed lymphocytes directly from granulomas without additional stimulation to capture the functions that were occurring *in situ*, as granulomas contain *Mtb* antigens and live and dead bacilli, which can serve as forms of T cell stimulation (Gideon et al., 2019). We observed very low frequencies of pro-inflammatory cytokine expression by all lymphocytes at any time point, though there is a significantly higher frequency of cells expressing IFN-γ and TNF in original granulomas from the early time point when compared with the mid and late time points (Figure S4A). Using markers that indicate activation, we observed the highest frequency of $CD69^+$ lymphocytes at the early time point and the inverse for expression of PD-1 (Figure S4A) (Freeman et al., 2000; Ziegler et al., 1994; Cibrián and Sánchez-Madrid, 2017). This temporal expression of activation markers was similar in $CD3^+$ subsets, with PD-1 expression being highest at the late time point and CD69 at the early or mid time points (Figure S4B). The $CD4^+$ and $CD8^+$ adaptive T cells showed very low frequencies of IFN-γ and TNF, with slightly higher frequencies occurring at the early and mid time points for $CD4^+$ T cells (medians: early, 1.49%; mid, 1.52%; late, 0.25%) (Figure S4B). Notable was the high frequency of IFN-γ and TNF production from $CD3^-CD20^-$ cells at the early time point (medians: IFN-γ, 16.85%; TNF, 8.72%), emphasizing their early innate function (Figure S4C).

To provide additional insight into the function of granuloma cells, we used flow cytometry to identify populations of TF-positive lymphocytes. The TFs assessed were GATA3, T-bet, Foxp3, RORa, and RORγT, which are regulators of cell differentiation and lineage commitment during an immune response for lymphoid cells (Moharrami et al., 2018; Saini et al., 2018; Yates et al., 2004; Wang et al., 2012; Fang and Zhu, 2017). Boolean gating indicated that the majority of lymphocytes in original granulomas at all time points did not express any of the TFs investigated (Figure 3A). Nevertheless, there was a significant increase in single and double TF expression at the mid and late time points post-infection (Figure 3A). When assessing only single TF expression in lymphocytes in granulomas across time points, there were statistically significant differences in all TFs investigated (Figures 3B and 3C). Although levels of Foxp3 and RORγT were very low at all time points, levels of RORα, GATA3, and T-bet were more substantial (Figures 3B and 3C).

Further analysis revealed that TF expression was dependent on the lymphocyte subset. Conventional $CD4^+$ T cells had a significant increase in the proportion of single TF^+ cells in granulomas from the late time point (Figure S5A). Similarly, approximately 20% of $CD4^+CD8^+$ cells, which represent a subset of CD4 cells with a heightened activation profile, expressed a single TF at the early and mid time points but had significantly higher expression at the late time point (Figure S5B) (Diedrich et al., 2019; Clénet et al., 2017). This contrasts with $CD8^+$ T cells, which had a median of 12.95% single TF expression at the early time point, with significantly higher frequencies of single TF^+ cells at both the mid (median: 24.2%) and late (median: 25.3%) time points, revealing that increases in TF expression in $CD8^+$ T cells occur earlier in granulomas compared with $CD4^+$ cells (Figures 5A-5C). $CD3^+CD4^-CD8^-$ cells, which include NK T cells and some γδ T cells, had very low frequencies of single TF expression at the early time point and significantly higher frequencies at the mid and late time points, with a highest median expression of 29.9% at the mid time point, although this expression was animal dependent (Figure S5D). There was

a trend for higher single TF expression in B cells ($CD3^{-}CD20^{+}$) at the mid and late time points compared with the early time point, although this was driven primarily by one animal at the late time point (Figure S5E). Innate lymphocytes ($CD3^{-}CD20^{-}$ cells), however, had similar frequencies of cells with single-positive-TF expression at all time points (medians: 24.64%, 33.07%, and 25.35%) (Figure S5F). Conventional T cells ($CD4^{+}$, $CD4^{+}CD8^{+}$, and $CD8^{+}$) and B cells had significantly higher expression of two TFs at the late time point compared with the early and mid time points (Figures S5A-S5C and S5E).

To investigate specific TF expression within lymphocyte subsets, we compared single TF expression, keeping in mind the frequency of lymphocyte subsets in granulomas at each time point (number of granulomas assessed: early = 24, mid = 31, late = 33) (Figure 4A). Consistent with what was observed in all lymphocytes (Figure 3B), there were relatively low frequencies of individual TF expression in many of the lymphocyte subsets at the early time point, with highest frequencies of RORα $CD4^{+}$ T cells (Figures 3B, 3C, and 4B). Innate lymphocytes ($CD3^{-}CD20^{-}$) had moderate levels of T-bet expression (medians: 16.7%, 27.92%, and 21.61%) at all time points investigated (Figure 4B), suggesting that these cells play a role throughout infection. There was minimal TF expression in $CD20^{+}$ B cells at all time points investigated, with modest increases in the frequency of RORα and GATA3 at the late time point, though these changes appear to be animal dependent (Figure 4B). At the early time point, we observed a low frequency of T-bet within adaptive $CD3^{+}$ T cells (medians: $CD4^{+}$, 2.44%; $CD8^{+}$, 4.65%; $CD4^{+}CD8^{+}$, 7.5%) (Figure 4B). However, at 12 and 20 weeks post-infection, there was a 5-fold increase in T-bet expression in $CD8^{+}$ T cells (medians: 22.2% and 21.2%). In contrast, there was no significant increase in T-$bet^{+}CD4^{+}$ T cells (including $CD4^{+}$ T cells expressing CD8, i.e., $CD4^{+}CD8^{+}$) until 20 weeks post-infection (medians: $CD4^{+}$, 17.59%; $CD4^{+}CD8^{+}$, 21%) (Figure 4B) (Diedrich et al., 2019; Clénet et al., 2017). Although $GATA3^{+}CD4^{+}$ cells were rare in most granulomas, the proportions observed at the mid and late time points were modestly increased in some animals. While frequencies of cells expressing two TFs were low at all time points (<6% of lymphocytes; Figure 3A), we observed significant increases in the co-expression of T-bet^{+}RORα^{+} and T-$bet^{+}GATA3^{+}$ at the late time point compared with the early and mid time points (Figure S5G). Taken together, these data support an evolution of the adaptive T cell response in granulomas over time.

To validate the flow cytometry data for TF expression and to investigate the localization of these cells in granulomas, we used immunofluorescence staining of granuloma tissue sections from the early, mid, or late time points post-infection. In keeping with the low levels of TF expression in early granulomas (Figure 4B), we found few $CD3^{+}$ cells expressing RORα or GATA3 in granuloma tissue sections (Figures S6A and S6B). Although the frequency of $Foxp3^{+}$ cells was consistently low at all time points, we could detect Foxp3 expressing $CD3^{+}CD4^{+}$ T cells (designated by arrows) (Figure S6C). Using a mid time point granuloma, we identified $CD3^{+}$T-bet^{+} cells throughout the lymphocyte region as well as within clusters of $CD11c^{+}$ macrophages (macrophage region), suggesting a potential interaction between these cell types (Figure 5A). There was consistent nuclear localization of T-bet (designated by arrows), indicating an activated cellular phenotype (Figure 5A) (McLane et al., 2013).

TF-positive cells have higher frequencies of pro-inflammatory cytokines than TF-negative cells

To assess the functionality of the TF^+ cells, we compared the frequency of pro-inflammatory cytokine expression in TF^+ cells versus TF^- cells from the same sample (Figures 6A-6C). At all time points, $ROR\alpha^+$ or T-bet^+ $CD4^+$ and $CD4^+CD8^+$ T cells had higher frequencies of IFN-γ, TNF, and CD69 expression compared with TF^- cells, supporting that TF^+ cells are activated and functional (Figures 6A and 6B). T-bet^+CD4^+ and T-$bet^+CD4^+CD8^+$ T cells had a higher frequency of PD-1 at the mid and late time points, suggesting that these cells have a different activation profile than $ROR\alpha^+CD4^+$ cells at the early time point.

$CD8^+$ T cells showed very low frequencies of $cytokine^+$ cells at all time points. Despite this, TF^+CD8^+ cells exhibited higher frequencies of pro-inflammatory cytokines when compared with TF^-CD8^+ cells (Figure 6C). The expression of the activation marker CD69 was significantly higher in in TF^+CD8^+ cells at the early and late time points but was not significant at the mid time point, suggesting that cellular interactions may differ for these cells at the mid time point. Conversely, there is higher expression of PD-1 in TF^-CD8^+ T cells at these time points, further supporting that while these TF^+CD8^+ cells are activated, they may be differentially regulated at various time points post-infection. TF expression in conjunction with low frequencies of cytokine expression suggested that $CD8^+$ T cells are contributing to the granuloma environment through other functions, such as producing cytotoxic molecules. To investigate this, we stained a granuloma from 12 weeks post-infection, observing granzyme B localization within $CD3^+CD8^+$ cells (designated by arrows) (Figure 5B). We observed colocalization of granzyme B with $CD3^+$T-bet^+ cells in the same granuloma and in a late time point granuloma (arrows) (Figures 5B and S6D). The available CD8 and T-bet antibodies could not be used in tandem for staining, limiting the ability to directly identify granzyme B expression in $CD8^+$T-bet^+ cells, but, taken together, our data suggest that $CD3^+CD8^+$ cells expressing T-bet produce granzyme B at 12 weeks post-infection. Of note, we observed granzyme B staining within the caseum; although this was not associated with intact nuclei (DAPI), this may be a true signal, potentially suggesting that the caseum is a sink for granzyme B. The presence of granzyme B within the caseum was also observed in granulomas from the late time point but varied in abundance between granulomas (Figures 5B and S6D).

Frequency of T-bet^+ cells negatively correlates with granuloma bacterial burden

Granulomas can contribute to *Mtb* protection by promoting immune responses that kill or restrict bacterial replication; conversely, they may promote disease by supporting *Mtb* growth and dissemination. By analyzing snapshots of granulomas at different time points, we can begin unraveling specific immune elements that are associated with a reduction in bacterial burden. One striking difference between granulomas at 4 weeks versus those at 12 and 20 weeks is the presence of T-bet^+ T cells. Correlation analyses revealed a modest but significant negative correlation between the proportion of all T-bet^+ lymphocytes, $CD4^+$T-bet^+ cells, or $CD8^+$T-bet^+ cells and CFUs per granuloma (Figures 7A-7C). This association suggests that T-bet^+ lymphocytes are one contributor to the reduction in bacterial burden seen in granulomas at 12 and 20 weeks post-infection. In contrast, correlation analysis performed comparing the frequency of the other TFs investigated among lymphocytes and

CFUs per granuloma showed few significant and strong correlations, with the exception of GATA3 among both lymphocytes and $CD4^+$ T cells (Figure S7). We also observed a significant negative correlation between the frequency of PD-1 among $CD4^+$ T cells and CFUs per granuloma, suggesting that PD-1 activation or regulation in $CD4^+$ T cells may contribute to the decreased CFUs in granulomas at the mid and late time points (Figure S7B).

DISCUSSION

Understanding the process of bacterial restriction and containment in lung TB granulomas is critical for identifying new targets for vaccines and therapeutics. Here, we compared original granulomas, i.e., those that arise from initial infection as determined by PET CT, from three distinct time points (4, 12, and 20 weeks) post-infection in NHPs (Martin et al., 2017). These time points represent early infection (early), the beginning of infection control (mid), and late infection (late), respectively. This affords an opportunity for temporal analysis of granuloma structure, cellular composition, and function, providing insight into some of the immune components that contribute to a reduction in bacterial burden. By only including granulomas originally observed at 4 weeks post-infection, we could focus on investigating the development and evolution of these granulomas, as previous data showed that granulomas that arise upon initial infection and those that arise later differ with respect to immunological factors and bacterial killing (Gideon et al., 2022; Lin et al., 2014). Our results reveal that immune responses mediated by T-bet-expressing T cells are delayed in granulomas, supporting that adaptive immunity in granulomas evolves over time. The slow evolution of adaptive immunity likely contributes to the ease of establishment of *Mtb* infection and substantial growth of the pathogen in early granulomas, where one originating bacillus in a granuloma reaches ~10^5 CFUs by 4 weeks (Lin et al., 2014). This suggests that vaccine-mediated enhancement of $CD8^+$ T cell responses, in addition to $CD4^+$ T cell responses, and rapid recruitment to the airways and lung following infection could improve protection against infection and progressive disease. Recent reports of vaccine strategies using cytomegalo-virus (CMV)-producing *Mtb* antigens, or intravenous and mucosal bacille Calmette–Guérin (BCG), support this concept, as they induce strong $CD4^+$ and/or $CD8^+$ T cell responses in airways and lungs and induce robust protection against *Mtb* infection or disease in macaques (Darrah et al., 2020; Hansen et al., 2018; Dijkman et al., 2019).

Granuloma structure has been investigated in various animal models and in humans, revealing a wide range of histopathological features. In humans and NHPs infected with *Mtb*, granulomas are classified as having necrotic (caseous), fibrotic, non-necrotic, mineralized, scarring, cavitary, and suppurative phenotypes (Flynn et al., 2015; Flynn and Klein, 2011; Lin et al., 2014). Necrotic granulomas were the most observed phenotype among original granulomas in this study, regardless of time point post-infection; however, a range of granuloma structures were observed in original lesions at the mid and late time points, including the presence of fibrosis. Prior studies in NHPs have investigated the role fibrosis plays in granuloma healing and containment, which is consistent with the lower CFUs in original granulomas with fibrosis observed in this study (Warsinske et al., 2017).

There were no major differences in the proportion of lymphocytes or myeloid cells in granulomas at the different stages of infection. There was a higher frequency in myeloid cell expression of the integrins CD11c and CD11b that aid in adherence, migration, and phagocytosis at the early time point (Lukácsi et al., 2020). A similar trend was observed in the frequency of cells expressing the scavenger receptor CD163, a marker often observed on alveolar macrophages (Bharat et al., 2016). While there are several potential hypotheses for these differences, one possibility is that granulomas from distinct time points are comprised of different myeloid subsets, i.e., early granulomas have more neutrophils and alveolar macrophages and fewer epithelioid macrophages. This hypothesis is reasonable as studies investigating the early events in granuloma formation and pathogen clearance reveal involvement of alveolar macrophages and neutrophils in the phagocytosis of bacteria and in bacterial clearance, respectively (Cohen et al., 2018). Regarding myeloid cell functionality, in late granulomas, we observed modest frequencies of cells producing IFN-γ or IL-10. As levels of IL-10 are higher than IFN-γ, myeloid cells may be more anti-inflammatory at late time points, possibly modulating pathology or contributing to *Mtb* persistence (Redford et al., 2011).

It is generally accepted that T cells are critical for the control of *Mtb* through production of cytokines such as IFN-γ, although it is not the only mediator of protection, and additional T cell functions are likely to be of equal importance (de Martino et al., 2019; Gideon et al., 2015; Lin et al., 2012; Gallegos et al., 2011). In fact, vaccines that induce production of IFN-γ by $CD4^+$ T cells are not always successful in the prevention of TB in animal models or humans (Darrah et al., 2019, 2020; Verreck et al., 2009; Tameris et al., 2013; Abou-Zeid et al., 1997; Orr et al., 2015; Griffiths et al., 2016). Our objective was to investigate lymphocytic phenotypes in granulomas at different time points not only for cytokine production but also for broader functionality using TFs. The role of TFs as lineage specifying among T cells has been well established, connecting the expression of T-bet, GATA3, Foxp3, RORα, and RORγT to T helper type 1 (T_H1), T_H2, regulatory T (T_{reg}), and T_H17 cells, respectively (Szabo et al., 2000; Ivanov et al., 2006; Zheng and Flavell, 1997; Hori et al., 2003). In granulomas, regardless of time point, the majority of lymphocytes were not expressing any of these TFs. One possible explanation for the low levels of TF expression is that lymphocytes in granulomas rarely encounter antigen-presenting cells infected with *Mtb* due to the spatial localization of cells in the granuloma, which has been predicted in previous studies using mathematical modeling (Millar et al., 2020). Another hypothesis is that many of the lymphocytes in granulomas are not specific for *Mtb* but migrate to the granuloma due to inflammatory signals and chemokines from infected or activated cells (Gideon et al., 2015; Wong et al., 2018; Millar et al., 2020). The necessity and function of adaptive T cell recruitment to *Mtb*-infected lungs has been investigated using various models, with studies in mice highlighting the roles of IL-23 and IL-17 as critical in the early recruitment of functional T cells to the lungs (Marino et al., 2011; Millar et al., 2020; Kauffman et al., 2018; Domingo-Gonzalez et al., 2017; Khader et al., 2007). While contributing events in the evolution of the adaptive immune response are not fully understood, bacterial reduction likely depends on spatially positioned, functional T cells for interaction with infected macrophages, as observed here with T-bet^+ cells in granulomas at 12 and 20 weeks post-infection.

At 4 weeks, we observed two pronounced phenotypes: (1) production of IFN-γ and TNF by innate lymphocytes and (2) RORα expression in lymphocytes. RORα is a member of the retinoid orphan receptor family and is canonically known for its role in the development of innate lymphoid cells (ILCs) and T_H17 cells (Yang et al., 2008; Ferreira et al., 2021; Lo et al., 2019). More recently, RORα was shown to be expressed in activated $CD4^+$ T cells of T_H1 and T_H2 helper cell lineages with relationships to chemotaxis and cell migration (Haim-Vilmovsky et al., 2021). Studies in *Mtb*-infected humans and mice also report an accumulation of ILCs in infected lungs and a protective role of ILC3s expressing the RORα homolog RORγT at early time points post-infection (Ardain et al., 2019). This suggests that innate lymphocytes as well as lymphocytes expressing ROR family proteins are vital cells in the early phases following *Mtb* infection, possibly for recruiting additional cells into the lung or granuloma, which facilitate bacterial killing at later time points.

At 12 weeks post-infection, there was a substantial increase in the frequency of T-bet expression in $CD8^+$ T cells followed by an increased frequency of $CD4^+$T-bet$^+$ cells at 20 weeks post-infection. The presence and role of T-bet has been investigated in the context of several infectious diseases, including TB, revealing its critical function in controlling infection through production of pro-inflammatory mediators, T cell trafficking, and inhibition of other T cell fates (Pritchard et al., 2019; Szabo et al., 2000; Sullivan et al., 2005; Lazarevic et al., 2013; Lord et al., 2005). The earlier temporal increase in T-bet$^+$$CD8^+$ T cells, which is coincident with a reduction in bacterial burden, suggests that these cells play a crucial role in bacterial control. This is consistent with our recent single-cell RNA sequencing (RNA-seq) data from NHP granulomas at 10 weeks post-infection (Gideon et al., 2022). Despite increases in T-bet$^+$$CD8^+$ cells at the mid and late time points, low frequencies of these cells produce pro-inflammatory cytokines. We instead observed granzyme B expression in these cells, suggesting a more traditional cytotoxic function. At the late time point, there are higher frequencies of $CD4^+$T-bet$^+$ and $CD4^+CD8^+$T-bet$^+$ cells producing IFN-γ or TNF and expressing PD-1 and CD69 when compared with T-bet$^-$ cells in the same granuloma. Surface expression of PD-1 is associated with activated cells or functional deficiency when co-expressed with other exhaustion markers, particularly in the context of cancer and viral infection (Barber et al., 2006; Dong et al., 2019). Studies in mice have identified an *Mtb*-specific subset of PD-1$^+$$CD4^+$ T cells that are functional and highly proliferative, potentially acting as a self-replenishing source of $CD4^+$ T cells in TB (Reiley et al., 2010). We have consistently observed low levels of cytokine production from T cells in NHP granulomas, which initially suggested an exhausted phenotype. However, we previously reported low levels of exhaustion markers on $CD3^+$ T cells and no difference in the cytokine production in cells with or without specific exhaustion markers (Wong et al., 2018). These studies, taken together, suggest that PD-1 expression in T-bet$^+$$CD4^+$ cells is likely related to T cell activation or regulation rather than exhaustion. Furthermore, our staining for T-bet$^+$ cells in granulomas showed nuclear localization of T-bet, which is indicative of an activated rather than exhaustive phenotype (McLane et al., 2013, 2021).

Limitations of the study

Though this study offers insight into the evolving granuloma environment, our flow cytometry panels for this experiment did not include antibodies to detect cytotoxic effector

molecules or additional TFs, which limited our ability to comprehensively assess immune responses in granulomas. Future studies will include the assessment of additional effector molecules with a focus on cytotoxic effectors such as granzymes and granulysin. In addition, applying single-cell RNA-seq on cells isolated from granulomas at distinct time points post-infection will provide a more robust and unbiased approach, corroborating the data provided herein. A recent study investigating both the functional and spatial components of human granulomas corroborates our findings, revealing an immunoregulatory macrophage phenotype within granulomas while also showing a low incidence of T cell exhaustion and activation (McCaffrey et al., 2022). We also recognize that the methods used in this paper for tissue dissociation may have altered the overall frequencies of specific cell types, including but not limited to Foxp3$^+$ T_{reg} cells. Our included immunohistochemical (IHC) data and other unpublished data in our lab suggest that the frequencies observed by flow cytometry for Foxp3$^+$ cells presented here are lower than anticipated.

In this study, early granulomas were characterized as having higher CFUs accompanied by higher frequencies of innate lymphocytes producing inflammatory cytokines and lower frequencies of adaptive lymphocytes expressing T-bet or any of the TFs investigated. The increase in T-bet$^+$ CD8$^+$ T cells preceded the appearance of T-bet$^+$ CD4$^+$ T cells at the later time points. This suggests that 4 weeks post-infection is prior to the development of an adaptive immune response, whereas at 12 (CD8$^+$) and 20 (CD4$^+$ and CD8$^+$) weeks, functional adaptive lymphocytes appear in granulomas, highlighting the prolonged time frame needed for the development of a robust adaptive T cell response to *Mtb* (Mehra et al., 2010). When comparing original granulomas, the proportion of T-bet$^+$ lymphocytes, T-bet$^+$CD4$^+$ cells, and T-bet$^+$CD8$^+$ cells negatively correlated with bacterial burden, suggesting that conventional T cells (CD4$^+$ and CD8$^+$) expressing T-bet contribute to the reduction in bacterial burden in granulomas at mid and late time points. The reduction in bacterial burden also coincides with an increase in histologic pathologies relating to granuloma healing or resolution. Although the temporal presence of T-bet$^+$ adaptive lymphocytes is likely driven by host and pathogen factors, vaccines and host-directed therapies aimed at facilitating faster recruitment of these functional adaptive T cells to *Mtb*-infected lungs would likely promote bacterial control and containment of disease.

STAR★METHODS

RESOURCE AVAILABILITY

Lead contact—Further information and requests for resources and reagents should be directed to and will be fulfilled by the lead contact, JoAnne Flynn (joanne@pitt.edu).

Materials availability—This study did not generate new unique reagents.

Data and code availability—Raw data reported in this study is available upon request from the lead contact. This paper does not report original code. Any additional information required to reanalyze the data reported in this paper is available from the lead contact upon request.

EXPERIMENTAL MODELS AND SUBJECT DETAILS

Animals and *Mtb* infection—Eight adult cynomolgus macaques (*Macaca fasicularis*) were infected with a low dose (15–20) CFU of *Mtb* (Erdman strain) via bronchoscopic installation as previously described (Table S1) (Capuano et al., 2003). NHPs were monitored daily in the Biosafety Level 3 (BSL3) laboratory at the University of Pittsburgh in compliance with the University's Institutional Animal Care and Use Committee (IACUC). Prior to infection, animals were examined and placed in quarantine to evaluate health and confirm no prior *Mtb* infection. For pathology analysis and figures, banked control samples with corresponding PET CT scan data were used to supplement the animals dedicated to this study, with only original granulomas (i.e. those first observed on 4 week scans) being utilized (Table S2).

Ethics statement—All experiments, protocols, and care of animals were approved by the University of Pittsburgh School of Medicine Institutional Animal Care and Use Committee (IACUC). The Division of Laboratory Animal Resources and IACUC adheres to national guidelines established by the Animal Welfare Act (7 U.S. Code Sections 2131-2159) and the Guide for the Care and use of Laboratory Animals (Eighth Edition) as mandated by the U.S. Public Health Service Policy. Animals used in this study were housed in rooms with autonomously controlled temperature and provided enhanced enrichment procedures as previously described (Winchell et al., 2020).

METHOD DETAILS

FDG PET CT imaging—Following *Mtb* infection, longitudinal PET CT imaging was performed to identify original granulomas and track disease over time. NHPs were sedated and injected with a PET tracer, 2-deoxy-2-(^{18}F)Fluoro-D-glucose (FDG), and imaged using the Mediso MultiScan LFER 150 (Mediso, Budapest, Hungary) PET CT integrated preclinical scanner (White et al., 2017; Lin et al., 2013). Imaging was performed in accordance with biosafety and radiation safety requirements within the BSL3 facility at the University of Pittsburgh every 2–4 weeks beginning at 4 weeks post-infection until pre-determined animal endpoint. Scans were analyzed using OsiriX DICOM (Pixmeo, Geneva, Switzerland) viewer software by in-house trained PET CT analysts (Pauline Maiello, H. Jacob Borish, and Alexander G. White) (White et al., 2017; Rosset et al., 2004).

Necropsy—Necropsy procedures were performed as previously described (Lin et al., 2009). In short, individual granulomas were identified using the pre-necropsy ^{18}F-FDG PET CT scan and isolated along with lymph nodes and portions of uninvolved lung lobes. At necropsy, NHPs were sedated with ketamine, maximally bled and humanely euthanized using pentobarbital and phenytoin (Beuthanasia; Schering-Plough, Kenilworth, NJ). To assess gross pathology, animals were scored based on number, size, and pattern of lung granulomas and extent of disease involvement in lobes, mediastinal LNs, and visceral organs as previously described (Lin et al., 2009). Tissues were bisected and placed in formalin for paraffin embedding to perform histological evaluation. Single-cell suspensions were obtained for assessment of bacterial burden and immunological assays using gentle macs enzymatic dissociation (59% of samples) or physical homogenization. Bacterial burden was evaluated for individual tissue sections by plating serial dilutions of homogenate on 7H11

or PANTA agar plates and incubated at 37°C in 5%CO_2 for 21 days. Total thoracic CFU is calculated from the summation of all lung, lung granuloma, and thoracic LN-plated samples (Maiello et al., 2017).

Flow cytometry—Following processing, single cell suspensions underwent surface and TF/intracellular cytokine staining (ICS). Prior to staining, cells were incubated at 37°C in 5% CO_2 in RPMI supplemented with 1%HEPES, 1% L-glutamine, 10% human AB serum, and 0.1% brefeldin A (Golgiplug; BD Biosciences, San Jose, CA) for 3 h. Cells were stained with a viability dye (Zombie NIR) followed by surface stains (Table S3) using standard protocols. TF and ICS was performed following permeabilization using True-Nuclear buffer kit according to the recommended protocol (True-Nuclear Transcription Factor Buffer Set; BioLegend, San Diego, CA). Samples were acquired on a Cytek Aurora (Cytek, Bethesda, MD) and analyzed using FlowJo Software (BD Biosciences) (Figure S2) and positive staining was verified against unstained controls. Only samples with >50 flow events in the parent population were reported. For analysis of $CD3^{-}CD20^{-}$ or $CD20^{+}$ cells, animal 6319 was excluded due to poor staining with the anti-CD20 antibody. In total, 88 granuloma samples were taken for flow cytometric analysis (early = 24, mid = 31, and late = 33) representing 94% (average) of the original lung granulomas isolated from animals at the time of necropsy (Table S2).

Histology—Individual tissue samples were formalin fixed paraffin embedded (FFPE) and cut into 5μm serial sections for histological evaluation. A veterinary pathologist (Edwin Klein) visually assessed the hematoxylin and eosin-stained lesions and described the histopathologic features and relevant cell types in each granuloma. Granuloma descriptions were categorized based on similar histopathologic description and analyzed to determine frequencies and presence of pathologic descriptors at each time point. Banked sections from animals with >3 granulomas having histologic descriptions were included for analyses.

Immunofluorescence—Cut and mounted FFPE tissue sections were treated with xylenes twice, 5 min each, followed by graded ethanol (95%, 70%) incubations for deparaffinization. Slides were subsequently boiled with antigen retrieval buffer (Tris-EDTA, pH9, made in house or citrate buffer, pH6, Sigma C999-1000mL) and blocked for one hour with PBS containing 1% BSA. Following blocking, slides were incubated with primary antibodies (Table S3) for one hour at room temperature (RT) or 18 h at 4°C in a humidified chamber. Fluorochrome-conjugated anti-mouse, rat, or rabbit antibodies, purchased from Jackson ImmunoResearch (Jackson ImmunoResearch Laboratories, West Grove, PA) and Thermo Fisher (Thermo Fisher, Waltham, MA), were used for secondary labeling for one hour at RT in a humidified chamber. Coverslips were mounted using ProLong Gold Antifade Mounting Medium with DAPI (Thermo Fisher) and imaged using an Olympus FV1000 confocal microscope (Olympus, Center Valley, PA) or Nikon e1000 (Nikon, Melville, NY) epifluorescent microscope. Post processing, images obtained on the Olympus confocal were stitched in Photoshop (Adobe Systems, Mountain View, CA) and images taken from both microscopes were brightened by applying a linear adjustment to the histogram levels for all channels in the entire image, taking care to maintain the integrity of the original image. Table S4 lists granulomas used for immunofluorescent analysis designated by figure.

QUANTIFICATION AND STATISTICAL ANALYSIS

Statistical analysis and transformations—Adjusted cell counts were determined based on the hemocytometer count at the time of tissue homogenization (cells/mL) multiplied by the total volume of the sample. This value was then adjusted for sample splitting (for staining controls) and cutting (roughly half sent for histology). Lastly, a limit of detection value (LOD) determined by total volume of sample was added to all samples to account for those that fall below detectable levels. Kruskal-Wallis tests were performed to determine if there were differences in necropsy time point followed by Dunn's multiple comparison tests to determine differences between specific groups. Non-parametric paired t tests were performed to compare frequencies of cytokine production from TF^+ cells and TF^- cells within the same sample. For all tests, p values < 0.05 were considered significant. CFU was log transformed (CFU+1/granuloma) to eliminate any zeroes from the analysis. Statistical analyses were performed using GraphPad Prism 9 (GraphPad Software, San Diego, CA).

Supplementary Material

Refer to Web version on PubMed Central for supplementary material.

ACKNOWLEDGMENTS

We thank Cassaundra Ameel, Carolyn Bigbee, Ryan Kelly, Amy Fraser, Janelle Gleim, Abigail Gubernat, Kush Patel, Mark Rodgers, and Jennie Vorhauer for their laboratory and technical assistance; Beth Junecko for imaging assistance; Chelsea Causgrove, Dan Fillmore, Kara Kracinovsky, Skyler Pergalske, and Jenn Sakal for veterinary assistance; and other members of the J.L.F., Scanga, and P.L.L. laboratories for their collaborative efforts and insightful conversations. This study was supported by a T32 training grant NIH 5T32AI1065380-13 and NIH AI123093 (J.L.F. and D.E.K.).

REFERENCES

Abou-Zeid C, Gares MP, Inwald J, Janssen R, Zhang Y, Young DB, Hetzel C, Lamb JR, Baldwin SL, Orme IM, et al. (1997). Induction of a type 1 immune response to a recombinant antigen from Mycobacterium tuberculosis expressed in Mycobacterium vaccae. Infect. Immun 65, 1856–1862. [PubMed: 9125572]

Ardain A, Domingo-Gonzalez R, Das S, Kazer SW, Howard NC, Singh A, Ahmed M, Nhamoyebonde S, Rangel-Moreno J, Ogongo P, et al. (2019). Group 3 innate lymphoid cells mediate early protective immunity against tuberculosis. Nature 570, 528–532. [PubMed: 31168092]

Barber DL, Wherry EJ, Masopust D, Zhu B, Allison JP, Sharpe AH, Freeman GJ, and Ahmed R (2006). Restoring function in exhausted CD8 T cells during chronic viral infection. Nature 439, 682–687. [PubMed: 16382236]

Barberis I, Bragazzi NL, Galluzzo L, and Martini M (2017). The history of tuberculosis: from the first historical records to the isolation of Koch's bacillus. J. Prev. Med. Hyg 58, E9–E12. [PubMed: 28515626]

Bharat A, Bhorade SM, Morales-Nebreda L, Mcquattie-Pimentel AC, Soberanes S, Ridge K, Decamp MM, Mestan KK, Perlman H, Budinger GRS, and Misharin AV (2016). Flow cytometry reveals similarities between lung macrophages in humans and mice. Am. J. Respir. Cell Mol. Biol 54, 147–149. [PubMed: 26274047]

Capuano SV 3rd, Croix DA, Pawar S, Zinovik A, Myers A, Lin PL, Bissel S, Fuhrman C, Klein E, and Flynn JL (2003). Experimental Mycobacterium tuberculosis infection of cynomolgus macaques closely resembles the various manifestations of human M. tuberculosis infection. Infect. Immun 71, 5831–5844. [PubMed: 14500505]

Cibrián D, and Sánchez-Madrid F (2017). CD69: from activation marker to metabolic gatekeeper. Eur. J. Immunol 47, 946–953. [PubMed: 28475283]

Clénet M-L, Gagnon F, Moratalla AC, Viel EC, and Arbour N (2017). Peripheral human CD4+CD8+ T lymphocytes exhibit a memory phenotype and enhanced responses to IL-2, IL-7 and IL-15. Sci. Rep 7, 11612. [PubMed: 28912605]

Cohen SB, Gern BH, Delahaye JL, Adams KN, Plumlee CR, Winkler JK, Sherman DR, Gerner MY, and Urdahl KB (2018). Alveolar macrophages provide an early Mycobacterium tuberculosis Niche and initiate dissemination. Cell Host Microbe 24, 439–446.e4. [PubMed: 30146391]

Coleman MT, Chen RY, Lee M, Lin PL, Dodd LE, Maiello P, Via LE, Kim Y, Marriner G, Dartois V, et al. (2014a). PET/CT imaging reveals a therapeutic response to oxazolidinones in macaques and humans with tuberculosis. Sci. Transl. Med 6, 265ra167.

Coleman MT, Maiello P, Tomko J, Frye LJ, Fillmore D, Janssen C, Klein E, and Lin PL (2014b). Early Changes by (18)Fluorodeoxyglucose positron emission tomography coregistered with computed tomography predict outcome after Mycobacterium tuberculosis infection in cynomolgus macaques. Infect. Immun 82, 2400–2404. [PubMed: 24664509]

Darrah PA, Difazio RM, Maiello P, Gideon HP, Myers AJ, Rodgers MA, Hackney JA, Lindenstrom T, Evans T, Scanga CA, et al. (2019). Boosting BCG with proteins or rAd5 does not enhance protection against tuberculosis in rhesus macaques. NPJ Vaccin. 4, 21.

Darrah PA, Zeppa JJ, Maiello P, Hackney JA, Wadsworth MH, Hughes TK, Pokkali S, Swanson PA, Grant NL, Rodgers MA, et al. (2020). Prevention of tuberculosis in macaques after intravenous BCG immunization. Nature 577, 95–102. [PubMed: 31894150]

de Martino M, Lodi L, Galli L, and Chiappini E (2019). Immune response to Mycobacterium tuberculosis: a narrative review. Front. Pediatr 7, 350. [PubMed: 31508399]

Diedrich CR, Gideon HP, Rutledge T, Baranowski TM, Maiello P, Myers AJ, and Lin PL (2019). CD4CD8 Double Positive T cell responses during Mycobacterium tuberculosis infection in cynomolgus macaques. J. Med. Primatol 48, 82–89. [PubMed: 30723927]

Dijkman K, Sombroek CC, Vervenne RAW, Hofman SO, Boot C, Remarque EJ, Kocken CHM, Ottenhoff THM, Kondova I, Khayum MA, et al. (2019). Prevention of tuberculosis infection and disease by local BCG in repeatedly exposed rhesus macaques. Nat. Med 25, 255–262. [PubMed: 30664782]

Domingo-Gonzalez R, Das S, Griffiths KL, Ahmed M, Bambouskova M, Gopal R, Gondi S, Muñoz-Torrico M, Salazar-Lezama MA, Cruz-Lagunas A, et al. (2017). Interleukin-17 limits hypoxia-inducible factor 1α and development of hypoxic granulomas during tuberculosis. JCI insight 2, e92973.

Dong Y, Li X, Zhang L, Zhu Q, Chen C, Bao J, and Chen Y (2019). CD4(+) T cell exhaustion revealed by high PD-1 and LAG-3 expression and the loss of helper T cell function in chronic hepatitis B. BMC Immunol. 20, 27. [PubMed: 31390978]

Fang D, and Zhu J (2017). Dynamic balance between master transcription factors determines the fates and functions of CD4 T cell and innate lymphoid cell subsets. J. Exp. Med 214, 1861–1876. [PubMed: 28630089]

Ferreira ACF, Szeto ACH, Heycock MWD, Clark PA, Walker JA, Crisp A, Barlow JL, Kitching S, Lim A, Gogoi M, et al. (2021). RORα is a critical checkpoint for T cell and ILC2 commitment in the embryonic thymus. Nat. Immunol 22, 166–178. [PubMed: 33432227]

Flynn JF, and Klein E (2011). In Pulmonary Tuberculosis in Monkeys. A Color Atlas of Comparative Pulmonary Tuberculosis Histopathology, Leong J, Datois V, and Dick T, eds. (Taylor and Francis Publishers).

Flynn JL, Chan J, and Lin PL (2011). Macrophages and control of granulomatous inflammation in tuberculosis. Mucosal Immunol. 4, 271–278. [PubMed: 21430653]

Flynn JL, Gideon HP, Mattila JT, and Lin PL (2015). Immunology studies in non-human primate models of tuberculosis. Immunol. Rev 264, 60–73. [PubMed: 25703552]

Freeman GJ, Long AJ, Iwai Y, Bourque K, Chernova T, Nishimura H, Fitz LJ, Malenkovich N, Okazaki T, Byrne MC, et al. (2000). Engagement of the PD-1 immunoinhibitory receptor by a novel B7 family member leads to negative regulation of lymphocyte activation. J. Exp. Med 192, 1027–1034. [PubMed: 11015443]

Gallegos AM, van Heijst JW, Samstein M, Su X, Pamer EG, and Glickman MS (2011). A gamma interferon independent mechanism of CD4 T cell mediated control of M. tuberculosis infection in vivo. PLoS Pathog. 7, e1002052. [PubMed: 21625591]

Gideon HP, Phuah J, Myers AJ, Bryson BD, Rodgers MA, Coleman MT, Maiello P, Rutledge T, Marino S, Fortune SM, et al. (2015). Variability in tuberculosis granuloma T cell responses exists, but a balance of pro- and anti-inflammatory cytokines is associated with sterilization. PLoS Pathog. 11, e1004603. [PubMed: 25611466]

Gideon HP, Phuah J, Junecko BA, and Mattila JT (2019). Neutrophils express pro- and anti-inflammatory cytokines in granulomas from Mycobacterium tuberculosis-infected cynomolgus macaques. Mucosal Immunol. 12, 1370–1381. [PubMed: 31434990]

Gideon HP, Hughes TK, Tzouanas CN, Wadsworth MH 2nd, Tu AA, Gierahn TM, Peters JM, Hopkins FF, Wei J-R, Kummerlowe C, et al. (2022). Multimodal profiling of lung granulomas in macaques reveals cellular correlates of tuberculosis control. Immunity, Apr 26:S1074-7613(22)00175-3. Epub ahead of print. 10.1016/j.immuni.2022.04.004.

Green AM, Difazio R, and Flynn JL (2013). IFN-γ from CD4 T cells is essential for host survival and enhances CD8 T cell function during Mycobacterium tuberculosis infection. J. Immunol 190, 270–277. [PubMed: 23233724]

Griffiths KL, Villarreal DO, Weiner DB, and Khader SA (2016). A novel multivalent tuberculosis vaccine confers protection in a mouse model of tuberculosis. Hum. Vaccin. Immunother 12, 2649–2653. [PubMed: 27322875]

Haim-Vilmovsky L, Henriksson J, Walker JA, Miao Z, Natan E, Kar G, Clare S, Barlow JL, Charidemou E, Mamanova L, et al. (2021). Mapping Rora expression in resting and activated CD4+ T cells. PLoS One 16, e0251233. [PubMed: 34003838]

Hansen SG, Zak DE, Xu G, Ford JC, Marshall EE, Malouli D, Gilbride RM, Hughes CM, Ventura AB, Ainslie E, et al. (2018). Prevention of tuberculosis in rhesus macaques by a cytomegalovirus-based vaccine. Nat. Med 24, 130–143. [PubMed: 29334373]

Hori S, Nomura T, and Sakaguchi S (2003). Control of regulatory T cell development by the transcription factor Foxp3. Science 299, 1057–1061. [PubMed: 12522256]

Ivanov II, Mckenzie BS, Zhou L, Tadokoro CE, Lepelley A, Lafaille JJ, Cua DJ, and Littman DR (2006). The orphan nuclear receptor RORgammat directs the differentiation program of proinflammatory IL-17+ T helper cells. Cell 126, 1121–1133. [PubMed: 16990136]

Kauffman KD, Sallin MA, Sakai S, Kamenyeva O, Kabat J, Weiner D, Sutphin M, Schimel D, Via L, Barry CE, et al. (2018). Defective positioning in granulomas but not lung-homing limits CD4 T-cell interactions with Mycobacterium tuberculosis-infected macrophages in rhesus macaques. Mucosal Immunol. 11, 462–473. [PubMed: 28745326]

Khader SA, Bell GK, Pearl JE, Fountain JJ, Rangel-Moreno J, Cilley GE, Shen F, Eaton SM, Gaffen SL, Swain SL, et al. (2007). IL-23 and IL-17 in the establishment of protective pulmonary CD4+ T cell responses after vaccination and during Mycobacterium tuberculosis challenge. Nat. Immunol 8, 369–377. [PubMed: 17351619]

Kumar P (2017). IFNγ-producing CD4(+) T lymphocytes: the double-edged swords in tuberculosis. Clin. Transl. Med 6, 21. [PubMed: 28646367]

Lazarevic V, Glimcher LH, and Lord GM (2013). T-bet: a bridge between innate and adaptive immunity. Nat. Rev. Immunol 13, 777–789. [PubMed: 24113868]

Lin PL, Rodgers M, Smith LK, Bigbee M, Myers A, Bigbee C, Chiosea I, Capuano SV, Fuhrman C, Klein E, and Flynn JL (2009). Quantitative comparison of active and latent tuberculosis in the cynomolgus macaque model. Infect. Immun 77, 4631. [PubMed: 19620341]

Lin PL, Rutledge T, Green AM, Bigbee M, Fuhrman C, Klein E, and Flynn JL (2012). CD4 T cell depletion exacerbates acute Mycobacterium tuberculosis while reactivation of latent infection is dependent on severity of tissue depletion in cynomolgus macaques. AIDS Res. Hum. Retrovir 28, 1693–1702. [PubMed: 22480184]

Lin PL, Coleman T, Carney JP, Lopresti BJ, Tomko J, Fillmore D, Dartois V, Scanga C, Frye LJ, Janssen C, et al. (2013). Radiologic responses in cynomolgus macaques for assessing tuberculosis chemotherapy regimens. Antimicrob. Agents Chemother 57, 4237–4244. [PubMed: 23796926]

Lin PL, Ford CB, Coleman MT, Myers AJ, Gawande R, Ioerger T, Sacchettini J, Fortune SM, and Flynn JAL (2014). Sterilization of granulomas is common in both active and latent tuberculosis despite extensive within-host variability in bacterial killing. Nat. Med 20, 75–79. [PubMed: 24336248]

Lo BC, Canals Hernaez D, Scott RW, Hughes MR, Shin SB, Underhill TM, Takei F, and Mcnagny KM (2019). The transcription factor RORα preserves ILC3 lineage identity and function during chronic intestinal infection. J. Immunol, ji1900781.

Lord GM, Rao RM, Choe H, Sullivan BM, Lichtman AH, Luscinskas FW, and Glimcher LH (2005). T-bet is required for optimal proinflammatory CD4+ T-cell trafficking. Blood 106, 3432–3439. [PubMed: 16014561]

Lukácsi S, Gerecsei T, Balázs K, Francz B, Szabó B, Erdei A, and Bajtay Z (2020). The differential role of CR3 (CD11b/CD18) and CR4 (CD11c/CD18) in the adherence, migration and podosome formation of human macrophages and dendritic cells under inflammatory conditions. PLoS One 15, e0232432. [PubMed: 32365067]

Maiello P, Difazio RM, Cadena AM, Rodgers MA, Lin PL, Scanga CA, and Flynn JL (2017). Rhesus macaques are more susceptible to progressive tuberculosis than cynomolgus macaques: a quantitative comparison. Infect. Immun

Marino S, El-Kebir M, and Kirschner D (2011). A hybrid multi-compartment model of granuloma formation and T cell priming in tuberculosis. J. Theor. Biol 280, 50–62. [PubMed: 21443879]

Martin CJ, Cadena AM, Leung VW, Lin PL, Maiello P, Hicks N, Chase MR, Flynn JL, and Fortune SM (2017). Digitally barcoding Mycobacterium tuberculosis reveals in vivo infection dynamics in the macaque model of tuberculosis. mBio 8, e00312–17. [PubMed: 28487426]

McCaffrey EF, Donato M, Keren L, Chen Z, Delmastro A, Fitzpatrick MB, Gupta S, Greenwald NF, Baranski A, Graf W, et al. (2022). The immunoregulatory landscape of human tuberculosis granulomas. Nat. Immunol 23, 318–329. [PubMed: 35058616]

McLane LM, Banerjee PP, Cosma GL, Makedonas G, Wherry EJ, Orange JS, and Betts MR (2013). Differential localization of T-bet and Eomes in CD8 T cell memory populations. J. Immunol 190, 3207–3215. [PubMed: 23455505]

McLane LM, Ngiow SF, Chen Z, Attanasio J, Manne S, Ruthel G, Wu JE, Staupe RP, Xu W, Amaravadi RK, et al. (2021). Role of nuclear localization in the regulation and function of T-bet and Eomes in exhausted CD8 T cells. Cell Rep. 35, 109120. [PubMed: 33979613]

Mehra S, Pahar B, Dutta NK, Conerly CN, Philippi-Falkenstein K, Alvarez X, and Kaushal D (2010). Transcriptional reprogramming in nonhuman primate (rhesus macaque) tuberculosis granulomas. PLoS One 5, e12266. [PubMed: 20824205]

Millar JA, Butler JR, Evans S, Mattila JT, Linderman JJ, Flynn JL, and Kirschner DE (2020). Spatial organization and recruitment of non-specific T cells may limit T cell-macrophage interactions within Mycobacterium tuberculosis granulomas. Front. Immunol 11, 613638. [PubMed: 33552077]

Moharrami NN, Bjørkøy Tande E, Ryan L, Espevik T, and Boyartchuk V (2018). RORα controls inflammatory state of human macrophages. PLoS One 13, e0207374. [PubMed: 30485323]

Okada S, Markle JG, Deenick EK, Mele F, Averbuch D, Lagos M, Alzahrani M, Al-Muhsen S, Halwani R, Ma CS, et al. (2015). Impairment of immunity to *Candida* and *Mycobacterium* in humans with bi-allelic *RORC* mutations. Science 349, 606–613. [PubMed: 26160376]

Orr MT, Windish HP, Beebe EA, Argilla D, Huang P-WD, Reese VA, Reed SG, and Coler RN (2015). Interferon γ and tumor necrosis factor are not essential parameters of CD4+ T-cell responses for vaccine control of tuberculosis. J. Infect. Dis 212, 495–504. [PubMed: 25637347]

Phuah J, Wong EA, Gideon HP, Maiello P, Coleman MT, Hendricks MR, Ruden R, Cirrincione LR, Chan J, Lin PL, and Flynn JL (2016). Effects of B Cell depletion on early *Mycobacterium tuberculosis* infection in cynomolgus macaques. Infect. Immun 84, 1301–1311. [PubMed: 26883591]

Pritchard GH, Kedl RM, and Hunter CA (2019). The evolving role of T-bet in resistance to infection. Nat. Rev. Immunol 19, 398–410. [PubMed: 30846856]

Redford PS, Murray PJ, and O'Garra A (2011). The role of IL-10 in immune regulation during M. tuberculosis infection. Mucosal Immunol. 4, 261–270. [PubMed: 21451501]

Reiley WW, Shafiani S, Wittmer ST, Tucker-Heard G, Moon JJ, Jenkins MK, Urdahl KB, Winslow GM, and Woodland DL (2010). Distinct functions of antigen-specific CD4 T cells during murine *Mycobacterium tuberculosis* infection. Proc. Natl. Acad. Sci. U S A 107, 19408. [PubMed: 20962277]

Rosset A, Spadola L, and Ratib O (2004). OsiriX: an open-source software for navigating in multidimensional DICOM images. J. Digit. Imag 17, 205–216.

Saini A, Mahajan S, Ahuja N, Bhagyaraj E, Kalra R, Janmeja AK, and Gupta P (2018). An accord of nuclear receptor expression in M. tuberculosis infected macrophages and dendritic cells. Sci. Rep 8, 2296. [PubMed: 29396519]

Sullivan BM, Jobe O, Lazarevic V, Vasquez K, Bronson R, Glimcher LH, and Kramnik I (2005). Increased susceptibility of mice lacking T-bet to infection with *Mycobacterium tuberculosis* correlates with increased IL-10 and decreased IFN-γ production. J. Immunol 175, 4593. [PubMed: 16177104]

Szabo SJ, Kim ST, Costa GL, Zhang X, Fathman CG, and Glimcher LH (2000). A novel transcription factor, T-bet, directs Th1 lineage commitment. Cell 100, 655–669. [PubMed: 10761931]

Tameris MD, Hatherill M, Landry BS, Scriba TJ, Snowden MA, Lockhart S, Shea JE, Mcclain JB, Hussey GD, Hanekom WA, et al. (2013). Safety and efficacy of MVA85A, a new tuberculosis vaccine, in infants previously vaccinated with BCG: a randomised, placebo-controlled phase 2b trial. Lancet 381, 1021–1028. [PubMed: 23391465]

Verreck FAW, Vervenne RAW, Kondova I, van Kralingen KW, Remarque EJ, Braskamp G, van der Werff NM, Kersbergen A, Ottenhoff THM, Heidt PJ, et al. (2009). MVA.85A boosting of BCG and an attenuated, phoP deficient M. tuberculosis vaccine both show protective efficacy against tuberculosis in rhesus macaques. PLoS One 4, e5264. [PubMed: 19367339]

Wang NS, Mcheyzer-Williams LJ, Okitsu SL, Burris TP, Reiner SL, and Mcheyzer-Williams MG (2012). Divergent transcriptional programming of class-specific B cell memory by T-bet and RORα. Nat. Immunol 13, 604–611. [PubMed: 22561605]

Warsinske HC, Difazio RM, Linderman JJ, Flynn JL, and Kirschner DE (2017). Identifying mechanisms driving formation of granuloma-associated fibrosis during Mycobacterium tuberculosis infection. J. Theor. Biol 429, 1–17. [PubMed: 28642013]

White AG, Maiello P, Coleman MT, Tomko JA, Frye LJ, Scanga CA, Lin PL, and Flynn JL (2017). Analysis of 18FDG PET/CT imaging as a tool for studying Mycobacterium tuberculosis infection and treatment in non-human primates. J. Vis. Exp 56375.

WHO (2020). In Global Tuberculosis Report 2020, W.H. ORGANIZATION, ed.

Winchell CG, Mishra BB, Phuah JY, Saqib M, Nelson SJ, Maiello P, Causgrove CM, Ameel CL, Stein B, Borish HJ, et al. (2020). Evaluation of IL-1 blockade as an adjunct to linezolid therapy for tuberculosis in mice and macaques. Front. Immunol 11, 891. [PubMed: 32477361]

Wong EA, Joslyn L, Grant NL, Klein E, Lin PL, Kirschner DE, and Flynn JL (2018). Low levels of T cell exhaustion in tuberculous lung granulomas. Infect. Immun 86, e00426–18. [PubMed: 29891540]

Yang XO, Pappu BP, Nurieva R, Akimzhanov A, Kang HS, Chung Y, Ma L, Shah B, Panopoulos AD, Schluns KS, et al. (2008). T helper 17 lineage differentiation is programmed by orphan nuclear receptors ROR alpha and ROR gamma. Immunity 28, 29–39. [PubMed: 18164222]

Yang R, Mele F, Worley L, Langlais D, Rosain J, Benhsaien I, Elarabi H, Croft CA, Doisne J-M, Zhang P, et al. (2020). Human T-bet governs innate and innate-like adaptive IFN-γ immunity against mycobacteria. Cell. 10.1016/j.cell.2020.10.046.

Yates A, Callard R, and Stark J (2004). Combining cytokine signalling with T-bet and GATA-3 regulation in Th1 and Th2 differentiation: a model for cellular decision-making. J. Theor. Biol 231, 181–196. [PubMed: 15380383]

Zheng W-P, and Flavell RA (1997). The transcription factor GATA-3 is necessary and sufficient for Th2 cytokine gene expression in CD4 T cells. Cell 89, 587–596. [PubMed: 9160750]

Ziegler SF, Ramsdell F, and Alderson MR (1994). The activation antigen CD69. Stem Cells 12, 456–465. [PubMed: 7804122]

Highlights

- T-bet expression in granuloma T cells increases over the course of *Mtb* infection
- T-bet^{+} T cells are inversely correlated with granuloma bacterial burden
- T-bet^{+} CD8 T cells appear in granulomas earlier than T-bet^{+} CD4 T cells

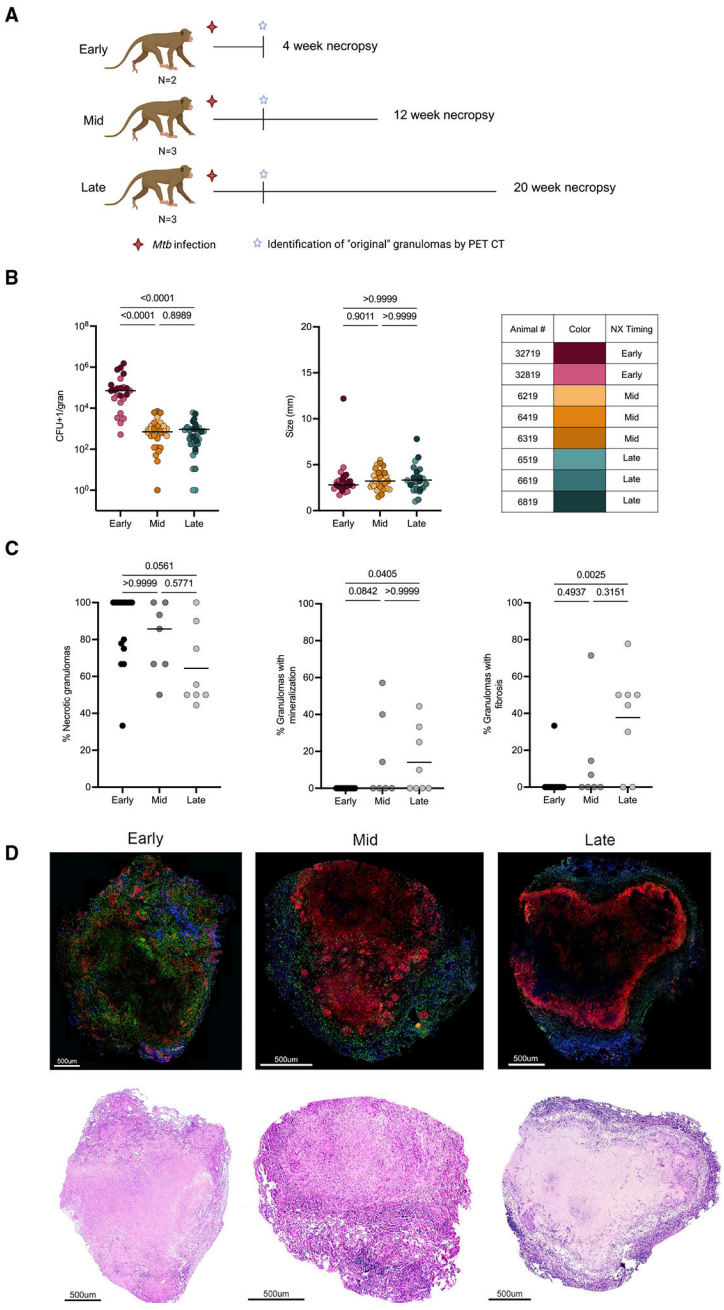

Figure 1. Study design, original granuloma dynamics, and pathology over time

(A) Eight Chinese cynomolgus macaques were infected with low-dose (10–19 colony-forming units [CFUs]) *Mtb* Erdman and followed for 4 (early), 12 (mid), or 20 (late) weeks post-infection. Original granulomas were defined as those first observed on the 4 weeks post-infection PET CT scan.

(B) Individual granuloma bacterial burden (CFUs) and size (mm) from PET CT. Individual points represent original lung granulomas (early: n = 24, mid: n = 31, late: n = 33). Table indicates each animal number and associated color in graphs.

(C) Histologic characteristics of original lung granulomas in individual animals (frequency of each granuloma type) of banked samples at early, mid, and late time points categorized by H&E descriptions. Data points represent individual animals (N = 14 early, 7 mid, and 8 late animals).

(D) Representative images of immunofluorescence staining for CD3 (green), CD11c (red), and CD163 (blue) with paired H&E staining of original granulomas from the early, mid, and late time points.

For (B) and (C) statistics, Kruskal Wallis tests were performed, with Dunn's multiple comparisons-adjusted p values reported on the graphs.

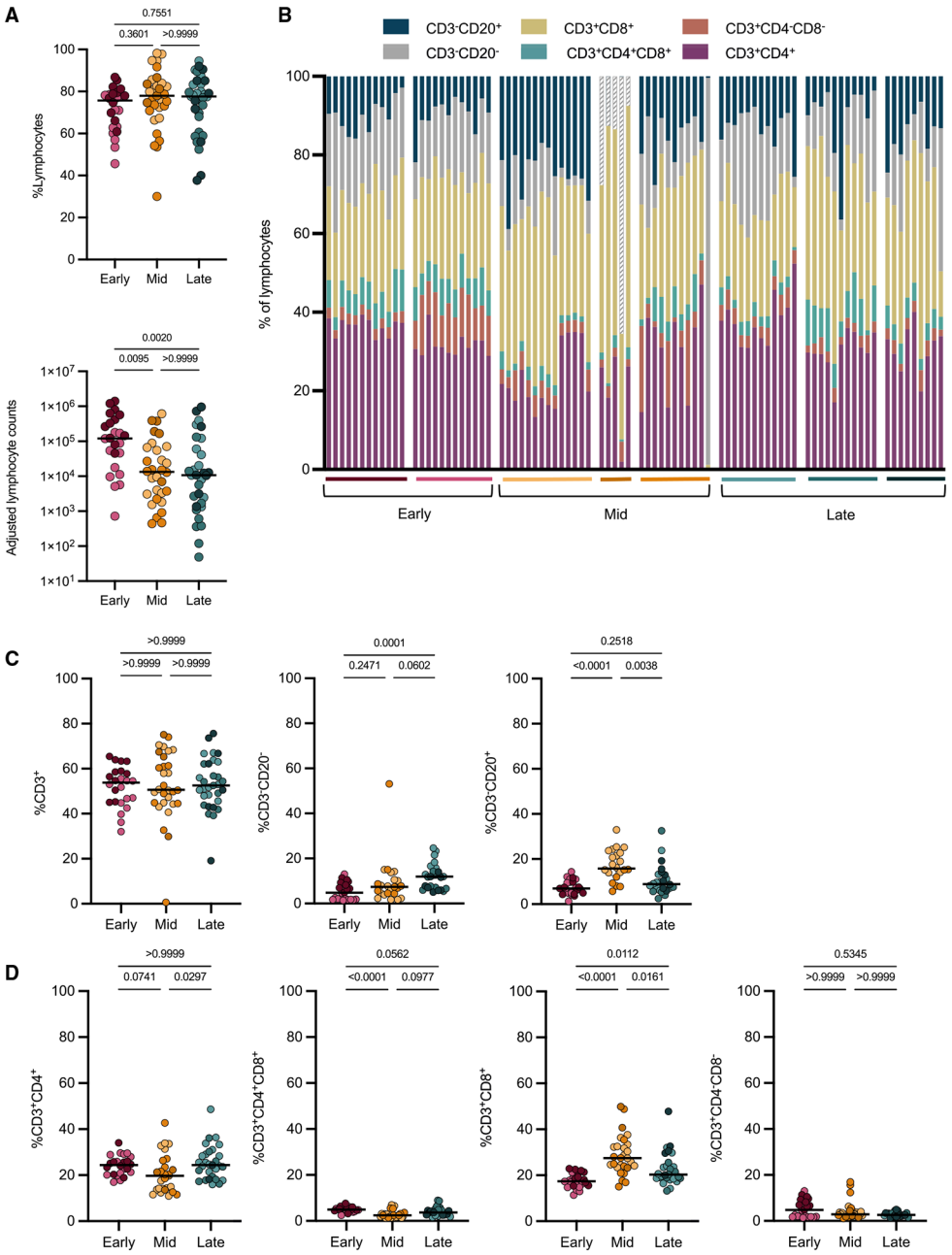

Figure 2. Few differences were observed in lymphocyte populations in original granulomas across time points

Original granulomas at each time point were evaluated for cellular composition by flow cytometry.

(A) Frequency (top) and numbers (bottom) of lymphocytes. Each symbol is a granuloma.

(B) Relative proportions of each cell type (percentage of lymphocytes) in individual granulomas. Each column is a granuloma and is separated by macaque (colored horizontal bar) and time point.

(C) Frequency of $CD3^+$, $CD3^-CD20^-$, and $CD3^-CD20^+$ of all live cells.

(D) Frequency of $CD4^+$, $CD4^+CD8^+$, $CD8^+$, and $CD4^-CD8^-$ of all live cells.

For (A), (C), and (D) statistics, Kruskal Wallis tests were performed, with Dunn’s multiple comparisons-adjusted p values reported on graphs.

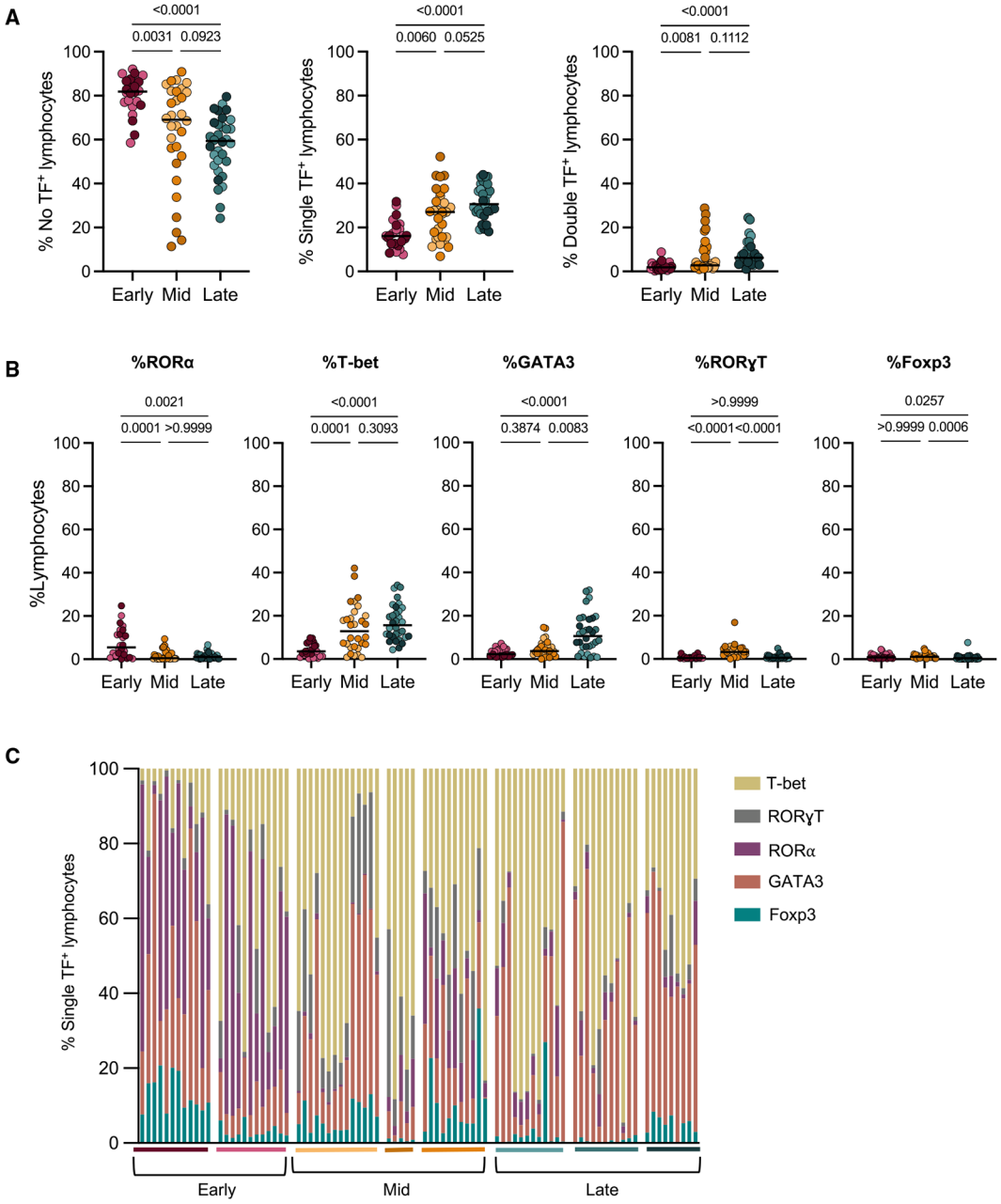

Figure 3. Temporal changes in transcription factor^{+} lymphocytes in original granulomas

(A) Original granulomas were assessed for transcription factor (TF) expression in lymphocytes via intracellular flow cytometry and were Boolean gated to determine frequency of single and double TF expression in lymphocytes.

(B) Frequency of lymphocytes expressing a single -TF from each time point. Individual symbols represent granulomas, which are colored according to animal (Figure 1B).

(C) Of the lymphocytes expressing a single TF, the relative proportion of each of the five TFs within individual granulomas is shown. Bars represent each granuloma, and animals are noted by the colored horizontal line and grouped by necropsy time point.

For (A) and (B) statistics, Kruskal Wallis tests were performed, with Dunn’s multiple comparisons-adjusted p values reported on graphs.

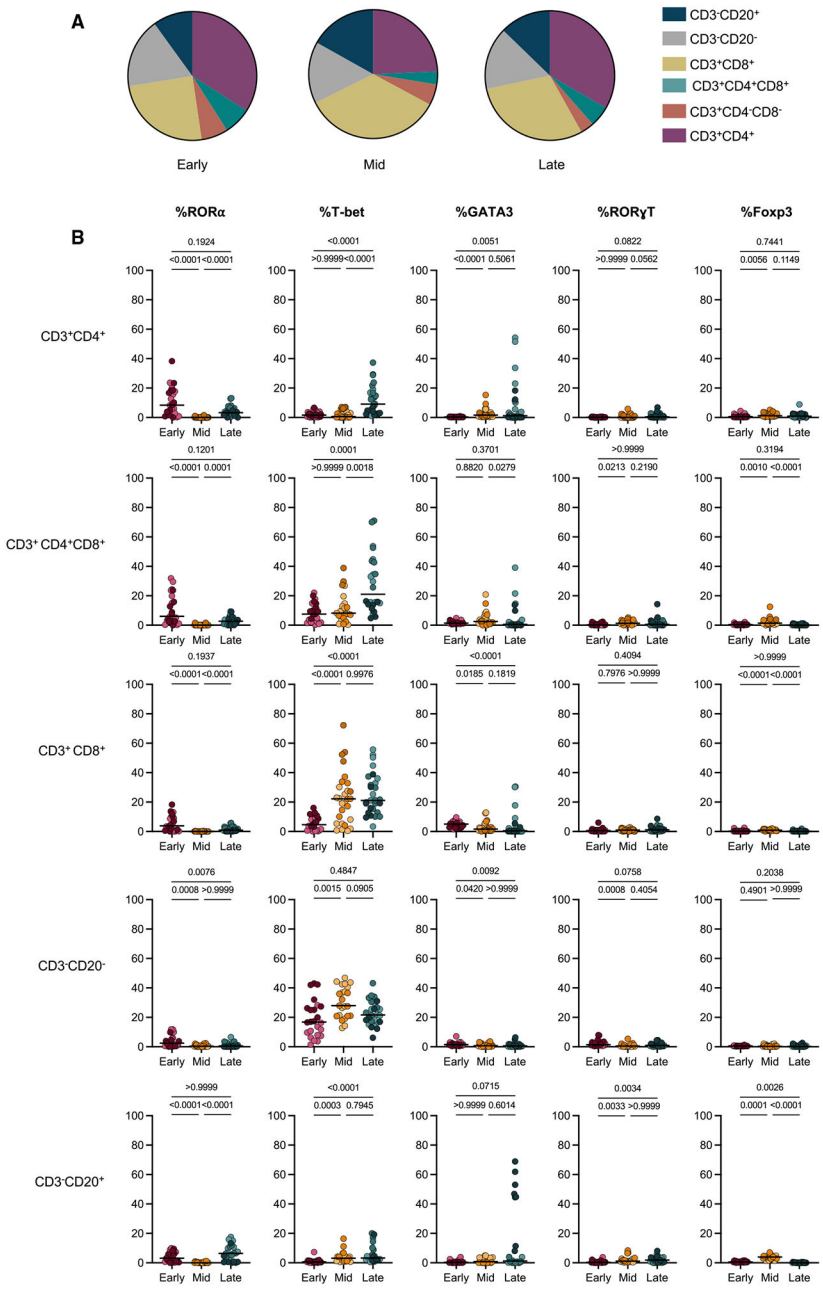

Figure 4. Delay in T-bet expression by conventional T cells in original granulomas

(A) Pie charts representing the average frequencies of denoted cell types (colored legend at right) from each time point (derived from Figure 2B).

(B) Frequencies of each single TF in lymphocyte subpopulations based on Boolean-gated flow cytometry data. Kruskal Wallis tests were performed, with Dunn's multiple comparisons-adjusted p values reported on graphs.

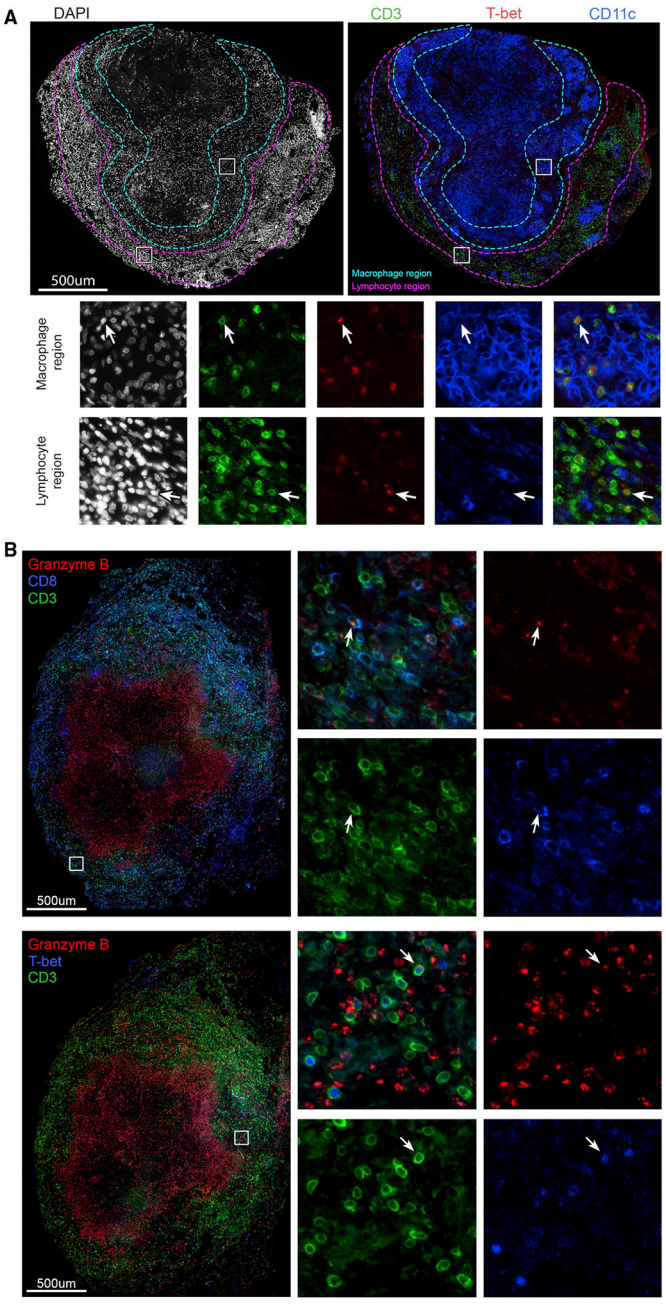

Figure 5. Presence, localization, and function of T-bet$^+$ lymphocytes in original granulomas

(A) Original granuloma from an animal 12 weeks post-infection with DAPI staining (left panel) and CD3 (green), T-bet (red), and CD11c (blue) staining (right panel). Insets as denoted in large image show localization of T-bet$^+$CD3$^+$ cells within macrophage regions (teal), as well as the lymphocyte cuff (magenta).

(B) Original granuloma isolated from an animal 12 weeks post-infection showing localization of granzyme B (red), in CD3$^+$ (green), and CD8$^+$(blue) cells (coregistered as teal and denoted with arrows; top panel) and CD3$^+$ (green) and T-bet$^+$ (blue) expressing granzyme B (red) (denoted by arrows; lower panel).

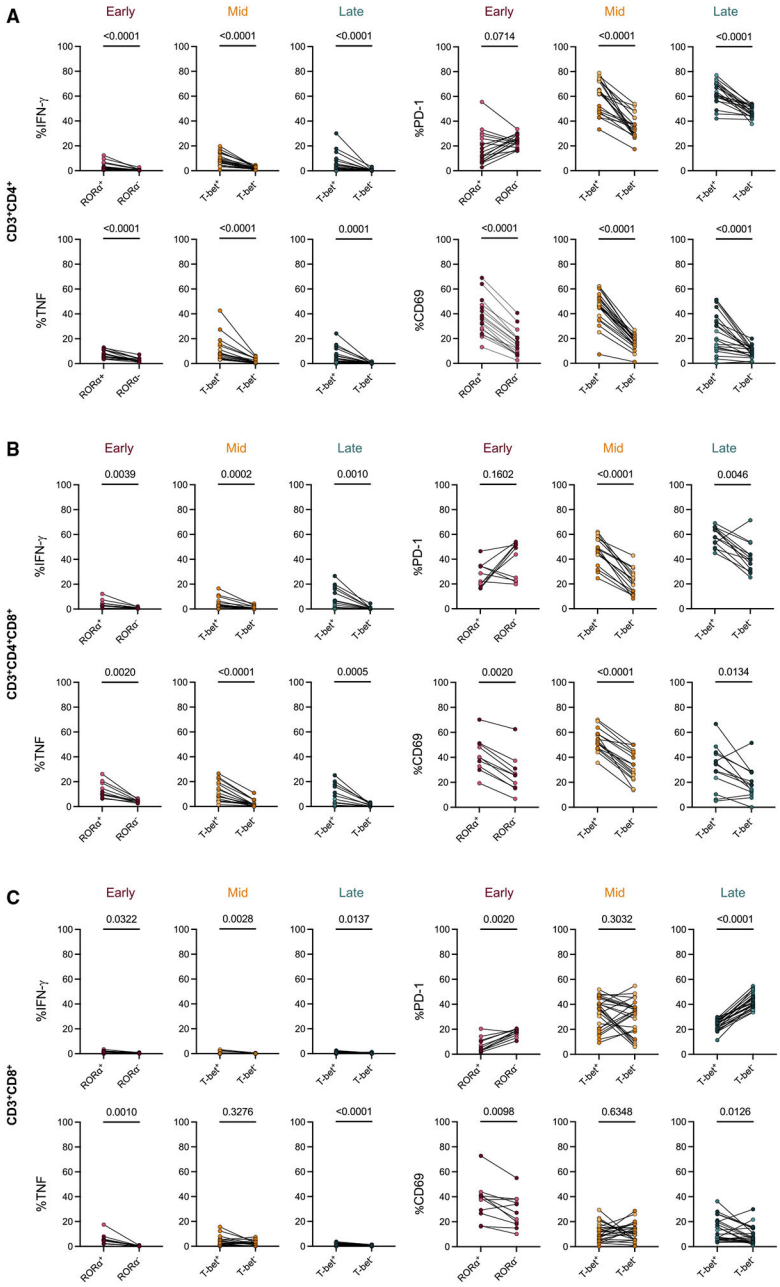

Figure 6. TF$^+$ cells produce more cytokines than TF$^-$ cells in original granulomas at all time points

(A–C) Comparison of pro-inflammatory cytokine (IFN-γ, TNF) production or activation marker (CD69, PD-1) expression in TF$^+$ T cells (RORα for early, T-bet for late) compared with TF$^-$ T cells for CD4$^+$ T cells (A), CD4$^+$CD8$^+$ T cells (B), and CD8$^+$ T cells (C). Samples were prepared by direct *ex vivo* staining in the absence of *in vitro* stimulation. All comparisons were performed using Wilcoxon signed-rank tests.

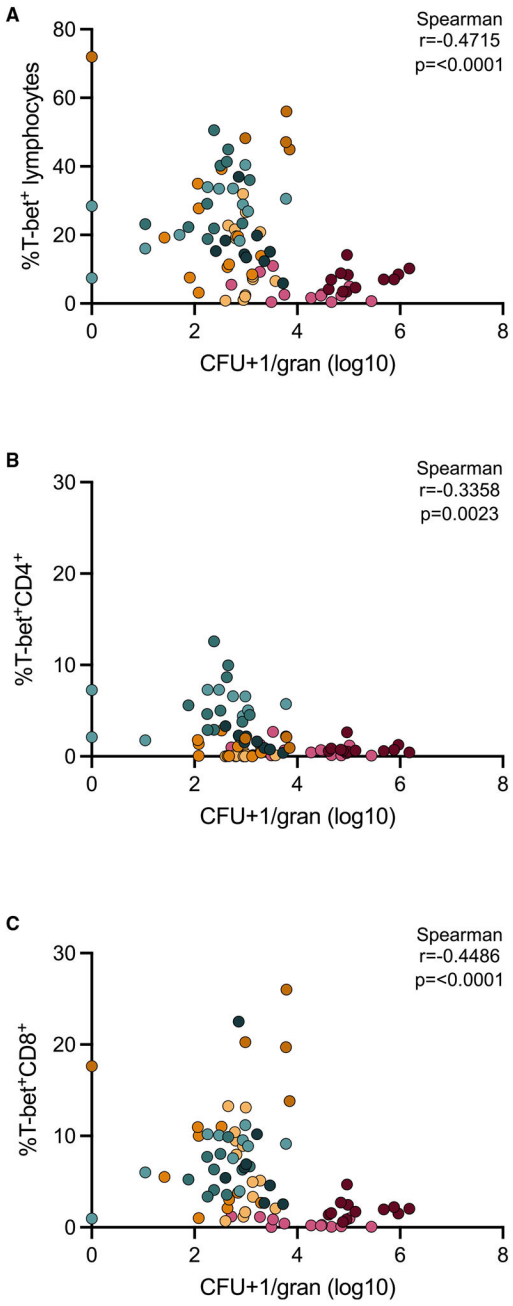

Figure 7. Bacterial burden negatively correlates with frequencies of T-bet$^+$ lymphocytes

(A) Frequency of T-bet$^+$ lymphocytes versus log10 CFUs per granuloma.

(B) Frequency of T-bet$^+$CD4$^+$ versus log10 CFUs per granuloma.

(C) Frequency of T-bet$^+$CD8$^+$ T cells versus log10 CFUs per granuloma. Data from all time points (early, mid, and late) are included in this analysis and colored according to animal (as previously indicated). CFUs per granuloma were log transformed after adding 1 (to avoid having undefined values). Non-parametric Spearman correlation analyses were performed, with rho and p values noted on individual graphs.

KEY RESOURCES TABLE

REAGENT or RESOURCE	SOURCE	IDENTIFIER
Antibodies		
See Table S3		
Bacterial and virus strains		
Mycobacterium tuberculosis (Erdman)	Passaged through mice, grown once in liquid culture, and frozen titered aliquots were made for infections.	no identifier
Chemicals, peptides, and recombinant proteins		
True-Nuclear Transcription Factor Buffer Set	BioLegend	Cat#424401
Experimental models: Organisms/strains		
Chinese Cynomolgus macaques	Valley Biosystems	no identifiers
Software and algorithms		
Prism v9	GraphPad	https://www.graphpad.com; RRID: SCR_002798
FlowJo v10	TreeStar	https://www.flowjo.com; RRID: SCR_008520